

Article

# Fatigue Life Assessment of Metals under Multiaxial Asynchronous Loading by Means of the Refined Equivalent Deformation Criterion

Daniela Scorza

Department of Engineering and Architecture, University of Parma, Parco Area delle Scienze 181/A, 43124 Parma, Italy; daniela.scorza@unipr.it

**Abstract:** As is well-known, non-proportional fatigue loading, such as asynchronous one, can have significant detrimental effects on the fatigue behavior of metallic materials by reducing the fatigue strength/fatigue limit and by leading to a fatigue damage accumulation increased with respect to that under proportional loading. In the present paper, the novel refined equivalent deformation (RED) criterion is applied for the first time to estimate the fatigue lifetime of materials, sensitive to non-proportionality, subjected to asynchronous loading under low-cycle fatigue regime. The present criterion is complete since it considers: (i) the strain path orientation, (ii) the degree of non-proportionality, and (iii) the changing of material cyclic properties under non-proportional loading. To evaluate its accuracy, this criterion is applied to examine two different metals (a 304 stainless steel and a 355 structural steel) whose experimental data under multiaxial asynchronous loading are available in the literature. More precisely, the parameters of the criterion are firstly determined by using experimental strain paths, and then the computed refined equivalent deformation amplitude is used to represent the experimental data with a satisfactory accuracy. Finally, a comparison with the results obtained through two other criteria available in the literature is performed, highlighting the good prediction of the present RED criterion.

**Keywords:** additional cyclic hardening; asynchronous loading; critical plane; LCF; non-proportional loading; RED criterion



**Citation:** Scorza, D. Fatigue Life Assessment of Metals under Multiaxial Asynchronous Loading by Means of the Refined Equivalent Deformation Criterion. *Metals* **2023**, *13*, 636. <https://doi.org/10.3390/met13030636>

Academic Editor: Yves Nadot

Received: 21 January 2023

Revised: 15 March 2023

Accepted: 17 March 2023

Published: 22 March 2023



**Copyright:** © 2023 by the author. Licensee MDPI, Basel, Switzerland. This article is an open access article distributed under the terms and conditions of the Creative Commons Attribution (CC BY) license (<https://creativecommons.org/licenses/by/4.0/>).

## 1. Introduction

It is well-known that non-proportionality of fatigue loading may have a significant influence on the fatigue behavior of metallic materials [1]. When loading components are not in constant proportion, that is, in the case of random components or in the case of periodical components phase-shifted and/or with different frequencies, the microstructure of metals may be strongly affected. As a matter of fact, the non-proportional changing of such loading components usually causes the rotation of the principal axes of stresses and strains, resulting in shear stresses acting in multiple directions and planes. Such shear stresses, indeed, may activate more slip systems compared with those activated under uniaxial and multiaxial proportional loading [2–4], producing: an increase of the dislocation interaction [5], a high density and a uniform distribution of the dislocations [3], the formation of dislocation cells of small sizes with great disorientation angles and great sharpness of cell walls [6,7]. As a result, an additional cyclic hardening of the material, as well as a reduction in the fatigue strength/fatigue limit, can be caused by the abovementioned dislocations mechanisms, leading to a fatigue damage accumulation increased with respect to that under proportional loading.

Consequently, the importance of considering the effect of loading non-proportionality from the points of view of both load analysis and material properties appears evident, although different materials show different susceptibilities to the same non-proportional loading degree [1]. For instance, a load characterized by a high degree of non-proportionality

acting on a material with a high susceptibility to non-proportionality can lead to a reduction in material fatigue strength of about ten times greater than that caused by a similar proportional loading [1,8]. Therefore, since such an effect cannot be underestimated in engineering practice, research on fatigue non-proportional loading condition is in continuous development [9–14].

Historically, the largest group of non-proportional loading used in fatigue tests is out-of-phase loading [15]. In such a case, the parameter that determines the degree of non-proportionality is the phase shift angle, which is constant over time. Another interesting group of non-proportional loading is the asynchronous one, where the loading components are characterized by different frequencies. In comparison with other cases of multiaxial loading, the results of fatigue tests conducted by using asynchronous loading are rarely published in the literature [16]. From such studies, it has been observed that the typical issues related to asynchronous loads are [16]:

- (i) the unclear cycle definition, due to different frequencies of the load components;
- (ii) the not obvious dependence of non-proportionality degree on the values of the ratio  $f_\gamma/f_\epsilon$  (being  $f_\gamma$  and  $f_\epsilon$  the frequencies of the shear and normal strain components, respectively);
- (iii) the existence of more than one plane where the maximum damage can be achieved (that is, multiple possible critical planes). For instance, in the case of both in-phase and out-of-phase loading, there are two planes of maximum shear strain and one plane of maximum normal strain, with the plane of maximum normal strain coincident with one of the two planes of maximum shear strain in the case of out-of-phase loading. On the contrary, in the case of asynchronous loading, the number of planes changes according to the  $f_\gamma/f_\epsilon$  ratio: for a butterfly-shape strain path ( $f_\gamma/f_\epsilon = 1/2$ ), four planes of maximum shear strain and two planes of maximum normal strain can be observed [16].

Therefore, it is worth noting that a fatigue criterion cannot accurately estimate fatigue life of components under asynchronous loading by only considering the stress/strain state inside a material for the computation of a suitable damage parameter. Among the criteria available in the literature for such an evaluation, both strain- and energy-based criteria are widely used [8,17–19]. In such a context, the novel refined equivalent deformation (RED) criterion [8,20] allows to take into account the effect of asynchronous loading on the fatigue strength for those materials sensitive to load non-proportionality. Such a RED criterion, already successfully applied in the case of out-of-phase loading [8,20], is applied here for the first time to analyze two experimental campaigns performed on 304 stainless steel and 355 structural steel components subjected to various asynchronous loading paths under multiaxial low cycle fatigue (LCF) regime [16].

The present paper is structured as follows. The experimental campaigns here examined are described in Section 2, whereas the RED criterion is presented in Section 3. Then, results and discussion are reported in Section 4. The main conclusions are summarized in Section 5.

## 2. Examined Experimental Campaigns

The examined experimental campaigns [16] are hereafter presented. More precisely, uniaxial and multiaxial fatigue tests under LCF regime were performed.

### 2.1. Materials and Specimens

The materials were 304 austenitic stainless steel (SS304, EN 1.4301), soft annealed, and non-alloy quality 355 structural steel (S355, EN 1.0580). The materials were purchased in the form of precise seamless pipes, and their mechanical properties are listed in Tables 1 and 2, respectively.

The above materials were selected since it is well known that they were characterised by a large additional cyclic hardening under non-proportional loading [16]. Note that, in Tables 1 and 2, the mechanical properties of both materials are reported, that is, the elastic

modulus,  $E$ , the yield strength,  $\sigma_y$ , and the effective Poisson's ratio,  $\nu_{eff}$ , together with the Manson-Coffin tensile and torsional parameters,  $\sigma'_f$ ,  $b$ ,  $\epsilon'_f$ ,  $c$  and  $\tau'_f$ ,  $b_0$ ,  $\gamma'_f$ ,  $c_0$ , respectively.

**Table 1.** Mechanical and fatigue properties of the 304 stainless steel (SS304) [20].

MATERIAL	$E$	$\sigma_y$	$\sigma'_f$	$b$	$\epsilon'_f$	$c$	$\tau'_f$	$G$	$b_0$	$\gamma'_f$	$c_0$	$\nu_{eff}$
	[GPa]	[MPa]	[MPa]	[-]	[-]	[-]	[MPa]	[GPa]	[-]	[-]	[-]	[-]
Ref.	[20]	[20]	[20]	[20]	[20]	[20]						[20]
SS304	183	550	1000	-0.114	0.171	-0.402	577	68.3	-0.114	0.296	-0.402	0.34

**Table 2.** Mechanical and fatigue properties of the 355 structural steel (S355) [16,21].

MATERIAL	$E$	$\sigma_y$	$\sigma'_f$	$b$	$\epsilon'_f$	$c$	$\tau'_f$	$G$	$b_0$	$\gamma'_f$	$c_0$	$\nu_{eff}$
	[GPa]	[MPa]	[MPa]	[-]	[-]	[-]	[MPa]	[GPa]	[-]	[-]	[-]	[-]
Ref.	[16]	[16]	[21]	[21]	[21]	[21]						[16]
S355	208.6	380	1001	-0.09	0.608	-0.616	578	79.0	-0.09	1.053	-0.616	0.29

Thin-walled tubular specimens were machined, whose sizes are shown in Figure 1.

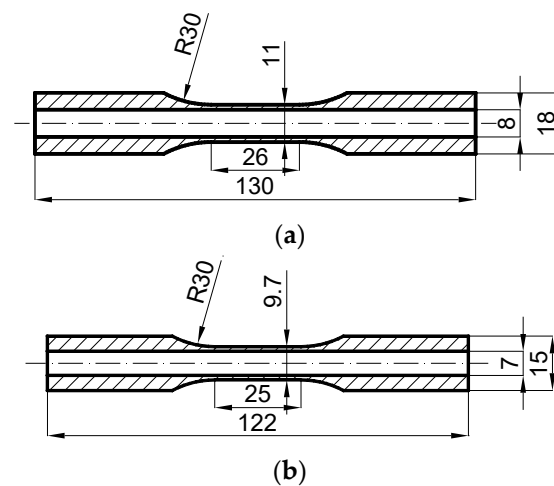


**Figure 1.** Geometry of the specimens made of (a) 304 stainless steel and (b) 355 structural steel (sizes in mm).

## 2.2. Testing Conditions and Experimental Results

All tests were performed by using an Instron 8874 axial-torsional closed-loop servo-hydraulic testing system under displacement control with a grip displacement velocity of 0.02 mm/s [16]. The axial and shear strains were measured by an Epsilon 3550 biaxial extensometer. The frequency of the fatigue tests was varied to keep the maximum value of the equivalent Huber–Mises strain rate below  $0.001 \text{ s}^{-1}$ , resulting in a frequency range from 2 Hz to tenths of Hz. Sine-shaped fully reversed waveforms of normal,  $\epsilon_z$ , and shear,  $\gamma_{zt}$ , strains were used, and their equations can be, respectively, written as:

$$\epsilon_z(t) = \epsilon_{z,a} \sin(2\pi f_\epsilon t) \quad (1a)$$

$$\gamma_{zt}(t) = \gamma_{zt,a} \sin(2\pi f_\gamma t + \beta) \quad (1b)$$

being  $\epsilon_{z,a}$ ,  $\gamma_{zt,a}$ ,  $f_\epsilon$  and  $f_\gamma$  the amplitudes and the frequencies of the normal and shear strains, respectively, and  $\beta$  the phase shift angle. Note that if  $f_\gamma/f_\epsilon = 1$ , a proportional (in-phase) loading takes place when  $\beta = 0^\circ$ , while a non-proportional out-phase loading is obtained for  $\beta \neq 0^\circ$ . On the other hand, if  $f_\gamma/f_\epsilon \neq 1$  for both  $\beta = 0^\circ$  and  $\beta \neq 0^\circ$ , the type

of loading is defined as asynchronous, with the normal and shear strain components not in constant proportion.

In both examined experimental campaigns [16], four synchronous loading conditions were considered as listed in Table 3, that is: tension–compression (TC), torsion (TOR), in-phase tension–torsion (IP), and out-of-phase tension–torsion (OP). Moreover, seven asynchronous loading cases (ASN) were considered, as detailed in Table 3. Note that  $\lambda$  is the ratio between the shear strain amplitude and the normal one ( $\lambda = \gamma_{zt,a}/\varepsilon_{z,a}$ ).

Table 3. Loading paths.

PATH	TC	TOR	IP	OP	ASN1	ASN2a	ASN2b	ASN3a	ASN3b	ASN4	ASN5
$\lambda = \gamma_{zt,a}/\varepsilon_{z,a}$	0	$\infty$	$\sqrt{3}$	$\sqrt{3}$	$\sqrt{3}$	$\sqrt{3}/2$	$\sqrt{3}$	$\sqrt{3}/2$	$2\sqrt{3}$	$3\sqrt{3}/5$	$\sqrt{3}$
$f_\gamma/f_\varepsilon$	-	-	1.00	1.00	0.50	4.00	4.00	0.20	0.25	6.00	0.70
$\beta[^\circ]$	-	-	0	90	0	0	0	0	0	0	0

The strain paths of the above synchronous and asynchronous loading in the  $\varepsilon_z$ - $\gamma_{zt}/\sqrt{3}$  plane are shown in Figure 2. Seven specimens were tested for each loading path (with the exception of loading paths IP, ASN2b and ASN3b for the S355 structural steel), in agreement with the ASTM E739 standard [22].

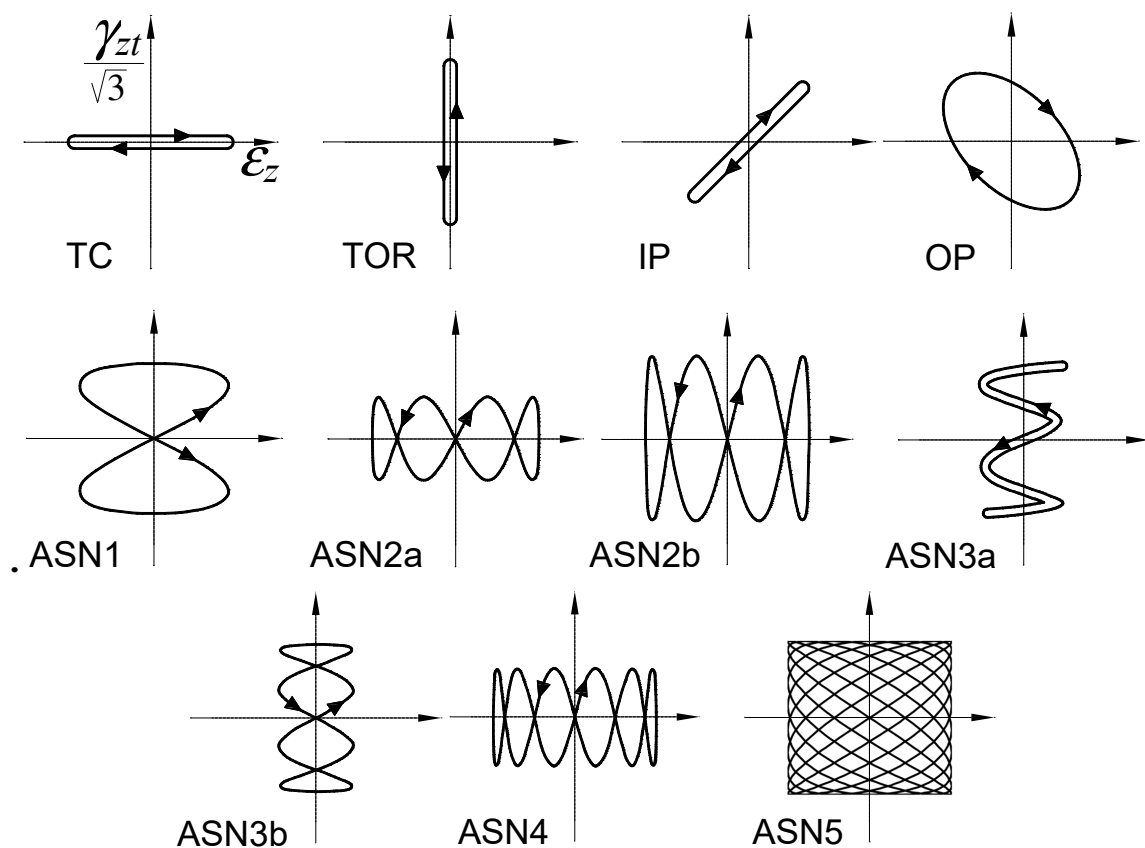


Figure 2. Strain paths examined [16] under proportional and non-proportional loading.

The failure condition was assumed to be reached when a 5% (or greater) drop in axial load or torque was observed (whichever occurred first) with respect to the corresponding value registered at approximately midlife [16]. Further details regarding the loading conditions can be found in Ref. [16].

The amplitudes  $\varepsilon_{z,a}$  and  $\gamma_{zt,a}$  of the applied strains are listed in Table 4 for the 304 stainless steel and in Table 5 for the 355 structural steel. Moreover, the experimental fatigue life,  $N'_{f,exp}$ , of all tested specimens is listed in Tables 4 and 5.

**Table 4.** 304 stainless steel: synchronous (left) and asynchronous (right) loading conditions and experimental fatigue life.

PATH	LOADING CONDITION	$\varepsilon_{z,a}$ [-]	$\gamma_{zt,a}$ [-]	$N'_{f,exp}$ [cycles]	PATH	LOADING CONDITION	$\varepsilon_{z,a}$ [-]	$\gamma_{zt,a}$ [-]	$N_{a,exp}$ [cycles]	$N_{t,exp}$ [cycles]	$N'_{f,exp}$ [cycles]
TC	1	0.0040	-	9457	ASN1	1	0.0028	0.0048	5969	2985	2985
	2	0.0050	-	2509		2	0.0032	0.0055	3184	1592	1592
	3	0.0055	-	1879		3	0.0040	0.0069	1019	510	510
	4	0.0060	-	1316		4	0.0044	0.0076	718	359	359
	5	0.0065	-	1133		5	0.0048	0.0083	736	368	368
	6	0.0070	-	875		6	0.0052	0.0090	448	224	224
	7	0.0080	-	561		7	0.0056	0.0097	429	215	215
TOR	1	-	0.0069	50,395	ASN2a	1	0.0033	0.0029	4645	18,580	4645
	2	-	0.0087	16,153		2	0.0038	0.0033	3026	12,104	3026
	3	-	0.0095	9270		3	0.0047	0.0041	1233	4930	1233
	4	-	0.0104	5920		4	0.0052	0.0045	1085	4338	1085
	5	-	0.0113	4760		5	0.0056	0.0049	492	1966	492
	6	-	0.0121	3445		6	0.0061	0.0053	604	2414	604
	7	-	0.0139	2874		7	0.0066	0.0057	412	1646	412
IP	1	0.0028	0.0049	14,255	ASN3a	1	0.0016	0.0054	53,656	10,731	10,731
	2	0.0035	0.0061	4136		2	0.0018	0.0062	29,099	5820	5820
	3	0.0039	0.0067	3624		3	0.0022	0.0077	10,708	2142	2142
	4	0.0042	0.0073	2440		4	0.0025	0.0085	6727	1346	1346
	5	0.0046	0.0080	1879		5	0.0027	0.0093	4711	942	942
	6	0.0049	0.0086	1370		6	0.0029	0.0101	4231	846	846
	7	0.0057	0.0098	969		7	0.0031	0.0108	2508	502	502
OP	1	0.0035	0.0061	2085	ASN4	1	0.0031	0.0032	5535	33,207	5535
	2	0.0040	0.0069	987		2	0.0035	0.0036	3550	21,297	3550
	3	0.0050	0.0087	622		3	0.0044	0.0046	1423	8535	1423
	4	0.0055	0.0095	388		4	0.0048	0.0050	933	5598	933
	5	0.0060	0.0104	325		5	0.0053	0.0055	727	4359	727
	6	0.0065	0.0113	246		6	0.0057	0.0059	586	3513	586
	7	0.0070	0.0121	170		7	0.0061	0.0064	353	2115	353
					ASN5	1	0.0025	0.0043	9130	6391	6391
						2	0.0028	0.0049	5551	3886	3886
						3	0.0036	0.0061	2141	1499	1499
						4	0.0039	0.0068	1506	1054	1054
						5	0.0053	0.0091	1298	909	909
						6	0.0046	0.0080	998	699	699
						7	0.0050	0.0086	687	481	481

**Table 5.** 355 structural steel: synchronous (left) and asynchronous (right) loading conditions and experimental fatigue life.

PATH	LOADING CONDITION	$\varepsilon_{z,a}$ [-]	$\gamma_{zt,a}$ [-]	$N'_{f,exp}$ [cycles]	PATH	LOADING CONDITION	$\varepsilon_{z,a}$ [-]	$\gamma_{zt,a}$ [-]	$N_{a,exp}$ [cycles]	$N_{t,exp}$ [cycles]	$N'_{f,exp}$ [cycles]
TC	1	0.0020	-	38,545	ASN1	1	0.0016	0.0028	12,815	6407	6407
	2	0.0030	-	7536		2	0.0020	0.0035	7101	3550	3550
	3	0.0040	-	5591		3	0.0024	0.0042	3269	510	510
	4	0.0050	-	3178		4	0.0028	0.0048	1730	359	359
	5	0.0060	-	1844		5	0.0032	0.0055	1565	782	782
	6	0.0070	-	1187		6	0.0040	0.0069	1162	581	581
	7	0.0080	-	850		7	0.0044	0.0076	789	215	215
TOR	1	-	0.0035	79,399	ASN2b	1	0.0026	0.0044	860	3440	860
	2	-	0.0052	11,207		2	0.0029	0.0051	951	3802	951
	3	-	0.0069	3061		3	0.0037	0.0063	484	1936	484
	4	-	0.0087	2833		4	0.0040	0.0070	423	1692	423
	5	-	0.0104	2439	ASN3b	1	0.0009	0.0033	31,987	7997	7997
	6	-	0.0121	1090		2	0.0014	0.0049	12,467	3117	3117
	7	-	0.0139	877		3	0.0016	0.0057	7859	1965	1965
IP	1	0.0021	0.0037	9683	4	0.0019	0.0065	6031	1508	1508	
	2	0.0028	0.0049	5863	5	0.0021	0.0073	5116	1279	1279	
	3	0.0035	0.0061	2992	6	0.0024	0.0081	3050	763	763	
	4	0.0042	0.0073	2316	ASN4	1	0.0018	0.0018	3559	21,354	3559
	5	0.0049	0.0086	1254		2	0.0022	0.0023	4881	29,283	4881
	6	0.0057	0.0098	991		3	0.0026	0.0027	1616	9693	1616
1	0.0019	0.0033	4697	4		0.0031	0.0032	950	5700	950	
2	0.0024	0.0042	1926	5		0.0035	0.0036	1302	7812	1302	
3	0.0029	0.0050	1576	6		0.0044	0.0046	530	3177	530	
OP	4	0.0034	0.0059	1351	7	0.0048	0.0050	602	3609	602	
	5	0.0039	0.0068	765	ASN5	1	0.0014	0.0025	21,803	15,262	15,262
	6	0.0049	0.0085	705		2	0.0018	0.0031	10,803	7562	7562
	7	0.0054	0.0094	402		3	0.0021	0.0037	6083	4258	4258
	4	0.0025	0.0043	3438		4	0.0025	0.0043	3438	2407	2407
	5	0.0028	0.0049	2428		5	0.0028	0.0049	2428	1700	1700
	6	0.0036	0.0061	1512		6	0.0036	0.0061	1512	1058	1058
7	0.0039	0.0068	1476	7		0.0039	0.0068	1476	1033	1033	

A particular mention is needed regarding the way such an experimental fatigue life  $N'_{f,exp}$  has been defined. As mentioned in the Introduction, one of the issues regarding the asynchronous loading is the unclear definition of a cycle, due to the different frequencies of the strain components. In the literature, two ways are usually followed to define such a fatigue life [16], that is: (i) the number of loading cycles to failure is taken equal to the number of cycles of the strain component with the lower frequency; or (ii) the fatigue life is assumed equal to the number of cycles performed by the strain components with higher frequency.

The most common approach is the first one [16], which is also the most conservative. Therefore, such an approach is followed also in this work, that is:  $N'_{f,exp} = \min(N_{a,exp}; N_{t,exp})$ , being  $N_{a,exp}$  and  $N_{t,exp}$  the number of loadings cycles to failure counted in the normal and shear strains channels during the experimental tests, respectively [16].

### 3. The Refined Equivalent Deformation (RED) Criterion

The RED criterion is a strain-based criterion that is based on the critical plane concept. The definition of the damage parameter,  $\varepsilon_{RED,a}$  (named refined equivalent deformation amplitude), introduced in Ref. [8], is in line with that employed by the Reduced Strain Range Method proposed by Borodii et al. [23–25]. Hereafter, a brief description of the criterion framework is given, whereas a detailed presentation of the criterion features can be found in Ref. [20].

#### 3.1. Material Sensitivity to Non-Proportional Loading

As mentioned in the Introduction, different metals have different sensitivities to non-proportional fatigue loading, that is, they react in different ways to a given fatigue loading characterized by a certain degree of non-proportionality. In order to take into account such an aspect, different parameters are available in the literature to quantify such a sensitivity to non-proportional fatigue loading [1], that is, for instance: the Stacking Fault Energy (SFE), the additional cyclic hardening coefficient,  $\alpha$ , and the ratio  $\tau_{af,-1}/\sigma_{af,-1}$  between the fully reversed shear strength and the fully reversed normal strength. By focusing the attention on the last one, that is the parameter used in the present criterion, it has been proved that a material is sensitive to non-proportional loading when  $\tau_{af,-1}/\sigma_{af,-1} \leq 1/\sqrt{3}$  [20]; therefore, in such a case, a possible decrease in fatigue strength/fatigue life has to be taken into account. On the other hand, when such a ratio is greater than  $1/\sqrt{3}$ , it is generally assumed that no effect produced by non-proportional loading has to be considered in the fatigue life assessment, and the criterion proposed in Ref. [26] can be directly applied.

#### 3.2. Critical Plane Determination

The critical plane  $\Delta$ , that is the plane where the fatigue assessment is performed, is determined according to the method proposed in Ref. [26]. Let us consider a biaxial fatigue loading, for which the strain tensor at a material point P located on the surface of a smooth engineering component has the following strain components:  $\varepsilon_r$ ,  $\varepsilon_t$ ,  $\varepsilon_z$ , and  $1/2\gamma_{zt}$  with respect to a fixed frame  $rtz$  (Figure 3).

The components  $\varepsilon_r$  and  $\varepsilon_t$  are functions of  $\varepsilon_z$  by means of the effective Poisson's ratio  $\nu_{eff}$ .

The principal strains  $\varepsilon_1$ ,  $\varepsilon_2$  and  $\varepsilon_3$  ( $\varepsilon_1 \geq \varepsilon_2 \geq \varepsilon_3$ ) and the corresponding directions are computed during the observation period  $T$  by identifying the instant when  $\varepsilon_1$  attains its maximum value during  $T$ . Its direction, named  $\hat{1}$ , is used to determine the normal  $\mathbf{w}$  to the critical plane: as a matter of fact,  $\mathbf{w}$  is assumed to form an angle  $\delta$  with respect to  $\hat{1}$ , where such a rotation is performed from  $\hat{1}$  to  $\hat{3}$ , being  $\hat{3}$  the direction of  $\varepsilon_3$  when  $\varepsilon_1$  is maximum. The angle  $\delta$  is computed as follows:

$$\delta = \frac{3}{2} \left\{ 1 - \left[ \frac{1}{2(1 + \nu_{eff})} \frac{\gamma_a}{\varepsilon_a} \right]^2 \right\} 45^\circ \quad (2)$$

where  $\epsilon_a$  and  $\gamma_a$  are computed according to the tensile and torsional Manson–Coffin equations, respectively:

$$\epsilon_a = \frac{\sigma'_f}{E} (2N_{f,cal})^b + \epsilon'_f (2N_{f,cal})^c \tag{3a}$$

$$\gamma_a = \frac{\tau'_f}{G} (2N_{f,cal})^{b_0} + \gamma'_f (2N_{f,cal})^{c_0} \tag{3b}$$

being  $\sigma'_f, b, \epsilon'_f, c$  and  $\tau'_f, b_0, \gamma'_f, c_0$  the parameters of the Manson–Coffin tensile and torsional equations, respectively, and  $N_{f,cal}$  the number of loading cycles.

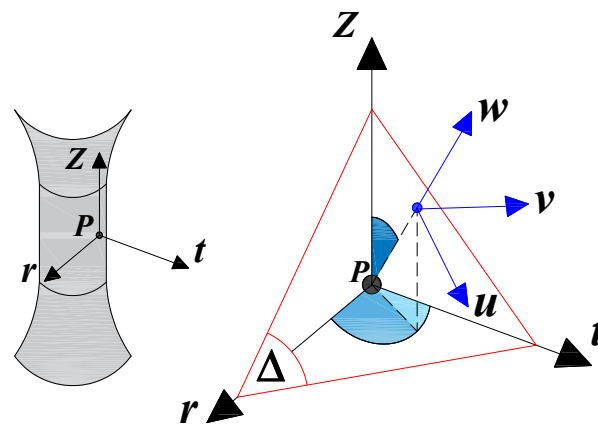


Figure 3. Global,  $rtz$ , and local,  $uvw$ , frames.

### 3.3. Damage Parameter Determination

Let us consider a local frame  $uvw$  (with origin at the abovementioned point  $P$ ) attached to the critical plane  $\Delta$  (Figure 3). The displacement  $\eta$  of the point  $P$  can be decomposed in a component  $\eta_N$ , function of the strain tensor component  $\epsilon_w$  along the normal to  $\Delta$ , and a component  $\eta_C$ , function of the strain tensor components  $\gamma_{wu}$  and  $\gamma_{wv}$  both lying on  $\Delta$ .

According to the RED criterion, the refined equivalent deformation amplitude,  $\epsilon_{RED,a}$ , is defined by the following equivalent deformation amplitude for non-proportional loading [8]:

$$\epsilon_{RED,a} = (1 + k \sin|45^\circ - \varphi_i|)(1 + \alpha \Phi_i) \epsilon_{eq,a}^p \tag{4}$$

where  $\epsilon_{eq,a}^p$  is the damage parameter for proportional loading, defined as [26]:

$$\epsilon_{eq,a}^p = \sqrt{(\eta_{N,a})^2 + \left(\frac{\epsilon_a}{\gamma_a}\right)^2 (\eta_{C,a})^2} \tag{5}$$

being  $\eta_{N,a}$  and  $\eta_{C,a}$  the amplitudes of  $\eta_N$  and  $\eta_C$ , respectively. Note that, having  $\eta_C$  different directions during the observation period, the maximum rectangular hull method [27] is used to compute  $\eta_{C,a}$ . Finally, the fatigue life,  $N_{f,cal}$ , is computed by iteratively solving the Equation (4), where  $\epsilon_{eq,a}^p$  is replaced by Equation (5).

It is worth noticing that Equation (5) is used even in the case of metals non sensitive to non-proportional loading: in such a case,  $k$  and  $\alpha$  are set equal to zero.

#### 3.3.1. $k$ and $\varphi_i$ Parameters Definitions

The parameter  $k$  is a material constant, which is representative of the material sensitivity to the change of fatigue properties, determined from uniaxial strain paths with respect to those determined from multiaxial proportional ones for the same strain amplitude. Such a constant is computed by considering only uniaxial strain paths:

$$k = \frac{1}{Q} \sum_{j=1}^Q k_j = \frac{1}{Q} \sum_{j=1}^Q \frac{1}{\sin 45^\circ} \left( \frac{\varepsilon_a(N'_{f,exp,j})}{\varepsilon_{eq,a}^p} - 1 \right) \quad (6)$$

where  $Q$  is the total number of uniaxial strain paths examined,  $\varepsilon_a(N'_{f,exp,j})$  is determined through the tensile Manson-Coffin equation (Equation (3a)) by replacing  $N_{f,cal}$  with the experimental number of loading cycles obtained for the  $j$ -th uniaxial strain path,  $N'_{f,exp,j}$ , whereas  $\varepsilon_{eq,a}^p$  is computed by means of Equation (5).

When  $k_j > 0$ , the material manifests sensitivity to the change of fatigue properties for the  $j$ -th strain path; on the contrary, when  $k_j \leq 0$ , the material does not manifest such a sensitivity, and  $k_j$  can be assumed equal to zero.

The parameter  $\varphi_i$  is the angle formed by the  $i$ -th non-proportional strain path with respect to the abscissa axis in the plane  $\varepsilon_z\text{-}\gamma_{zt}/\sqrt{3}$ . In order to measure such an angle, the direction of the  $i$ -th non-proportional strain path has to be determined. Such a direction is defined as the maximum length of the segment that joints two points on the strain path in the  $\varepsilon_z\text{-}\gamma_{zt}/\sqrt{3}$  plane, named  $\Delta\varepsilon_m$  in the following. Consequently,  $\varphi_i$  is measured between the above segment and the abscissa axis of the above plane [20].

### 3.3.2. $\alpha$ and $\Phi_i$ Parameters Definitions

The material constant  $\alpha$  is determined by only considering non-proportional strain paths [20]:

$$\alpha = \frac{1}{M} \sum_{i=1}^M \alpha_i = \frac{1}{M} \sum_{i=1}^M \frac{1}{\Phi_i} \left( \frac{\varepsilon_a(N'_{f,exp,i})}{\varepsilon_{eq,a}^p} - 1 \right) \quad (7)$$

being  $M$  the total number of the non-proportional strain paths examined,  $\varepsilon_a(N'_{f,exp,i})$  is determined through the tensile Manson-Coffin equation (Equation (3a)) by replacing  $N_{f,cal}$  with the experimental number  $N'_{f,exp,i}$  of loading cycles obtained for the  $i$ -th non-proportional strain path, and  $\varepsilon_{eq,a}^p$  is computed by means of Equation (5). The parameter  $\alpha$  is representative of the material sensitivity to non-proportional loading: when  $\alpha_i > 0$ , the material manifests the above sensitivity for the  $i$ -th strain path; on the contrary, when  $\alpha_i \leq 0$ , the material does not manifest such a sensitivity, and  $\alpha_i$  can be assumed equal to zero.

The parameter  $\Phi_i$  is the coefficient of non-proportionality related to the  $i$ -th non-proportional strain path and it is defined according to the method proposed by Borodii et al. [23–25], where a detailed description of its computation is given in Ref. [20]. Such a coefficient is defined as:

$$\Phi_i = \left( \frac{S_i}{S_{0,i}} \right)^{r_i} \quad (8)$$

When the non-proportional strain path in the  $\varepsilon_z\text{-}\gamma_{zt}/\sqrt{3}$  plane is a *closed strain path* (that is, a *convex path*),  $S_i$  is the area enveloped by the  $i$ -th convex path and  $S_{0,i}$  is the area of the smallest circle that contains the above path in the  $\varepsilon_z\text{-}\gamma_{zt}/\sqrt{3}$  plane. The exponent  $r_i$  is defined as:

$$r_i = 1 \quad \text{for smooth strain path} \quad (9a)$$

$$r_i = \left( 1 - \frac{S_i}{S_{0,i}} \right) \frac{l_i}{4\Delta\varepsilon_m} \quad \text{for piecewise broken line strain path} \quad (9b)$$

where  $l_i$  is the length of the convex path.

On the contrary, when the non-proportional strain path in the  $\varepsilon_z\text{-}\gamma_{zt}/\sqrt{3}$  plane is an *open strain path* (that is, a *non-convex path*),  $S_i$  is the area enveloped by an equivalent convex strain path containing the  $i$ -th one and  $S_{0,i}$  is the area of the smallest circle that contains the above equivalent path in the  $\varepsilon_z\text{-}\gamma_{zt}/\sqrt{3}$  plane. In such a case, the exponent  $r_i$  is given by:

$$r_i = \frac{l_i}{4\Delta\varepsilon_m} \quad (10)$$

where  $l_i$  is the length of the non-convex path.

#### 4. Results and Discussion

In the present section, the RED criterion is applied to simulate the results of the biaxial loading experimental tests described in Section 2.

##### 4.1. 304 Stainless Steel

##### 4.1.1. Material Sensitivity to Non-Proportional Loading and RED Parameter Computation

According to the present criterion, some input data have to be set, which are listed in Table 1 for the 304 stainless steel. More precisely, the values of  $\sigma'_f$ ,  $E$ ,  $b$ ,  $\varepsilon'_f$  and  $c$  are taken from Ref. [20], the Huber–Mises–Hencky hypothesis is assumed for both  $\tau'_f$  and  $\gamma'_f$ , that is,  $\tau'_f = \sigma'_f/\sqrt{3}$  and  $\gamma'_f = \varepsilon'_f/\sqrt{3}$ , respectively, as commonly suggested in the literature [28],  $b_0 = b$  and  $c_0 = c$  are assumed, and  $G$  is determined as a function of the elastic modulus  $E$ . The fatigue strengths  $\sigma_{af,-1}$  and  $\tau_{af,-1}$  are computed as follows:

$$\sigma_{af,-1} = \sigma'_f(2N_0)^b \quad (11a)$$

$$\tau_{af,-1} = \tau'_f(2N_0)^{b_0} \quad (11b)$$

By assuming  $N_0 = 2 \cdot 10^6$  loading cycles, such strengths are equal to 177 MPa and  $\tau_{af,-1} = \tau'_f(2N_0)^{b_0} 102$  MPa, respectively. The ratio  $\tau_{af,-1}/\sigma_{af,-1}$  is equal to 0.576, that is, the material is considered sensitive to non-proportional loading, being such a value slightly lower than  $1/\sqrt{3}$ . Further, also  $\nu_{eff}$  is taken from Ref. [20].

The computed values of  $k$  and  $\alpha$  for such a steel are equal to 0.3104 and 0.4814, respectively.

##### 4.1.2. Proportional Loading Tests Results

When loading components are in a constant proportion, such as in the case of the synchronous strain path IP where tension and torsion are in-phase, the damage parameter  $\varepsilon_{eq,a}^p$ , defined in Equation (5), is used [26]. Figure 4 shows the correlation between the experimental fatigue life,  $N'_{f,exp}$ , and the computed fatigue life,  $N'_{f,cal}$ .

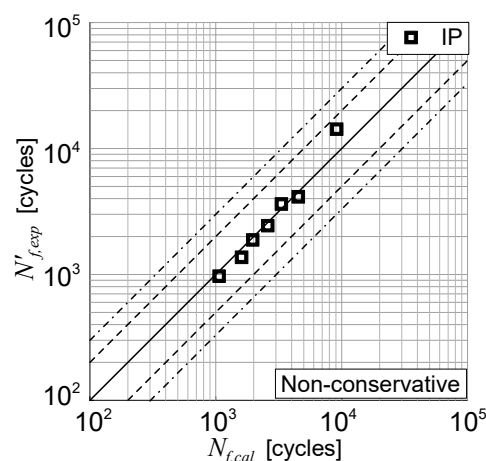


**Figure 4.** Correlation between the experimental fatigue life,  $N'_{f,exp}$ , of the 304 stainless steel specimens under proportional loading and the computational fatigue life,  $N'_{f,cal}$ .

As can be observed from Figure 4, all the results fall in scatter band 2 (defined by the dashed lines). The accuracy of the estimations is evaluated with the root mean square

(RMS) error method [26]. The root mean square error,  $T_{RMS}$ , is determined through the following relationship:

$$T_{RMS} = 10^{E_{RMS}} \quad (12)$$

where  $E_{RMS}$  related to fatigue lifetime is computed as follows:

$$E_{RMS} = \sqrt{\frac{\sum_{l=1}^{13} \log^2(T_{exp}/T_{cal})_l}{13}} \quad (13)$$

For the synchronous strain path IP  $T_{RMS}$  is equal to 1.21.

#### 4.1.3. Non-Proportional Loading Tests Results

The computed values of  $\varphi_i$  and  $\Phi_i$  are listed in Table 6 for each examined non-proportional loading condition. The computed values of both  $\varepsilon_{RED,a}$  and  $N_{f,cal}$  are also listed in such a table.

The correlation between the experimental fatigue life  $N'_{f,exp}$  and the non-proportional damage parameter,  $\varepsilon_{RED,a}$ , are shown in Figure 5a, whereas the correlation between the experimental fatigue life  $N'_{f,exp}$  and the damage parameter of Ref. [26],  $\varepsilon_{eq,a}^p$ , is shown in Figure 5b, together with the Manson-Coffin curves (see the black solid lines).

**Table 6.** 304 stainless steel:  $\varphi_i$ ,  $\Phi_i$ ,  $\varepsilon_{RED,a}$  and  $N_{f,cal}$  values for each examined non-proportional loading condition.

PATH	LOADING CONDITION	$\varphi_i$ [rad]	$\Phi_i$ [-]	$\varepsilon_{RED,a}$ [-]	$N_{f,cal}$ [cycles]
OP	1	2.37	0.62	0.0097	1207
	2	2.37	0.62	0.0110	840
	3	2.37	0.62	0.0138	431
	4	2.37	0.62	0.0151	336
	5	2.37	0.62	0.0165	262
	6	2.37	0.62	0.0179	206
	7	2.37	0.62	0.0192	171
ASN1	1	0.70	0.54	0.0071	3124
	2	0.70	0.54	0.0081	2074
	3	0.70	0.27	0.0091	1477
	4	0.70	0.55	0.0112	802
	5	0.70	0.54	0.0121	626
	6	0.70	0.54	0.0131	498
	7	0.70	0.54	0.0142	403
ASN2a	1	0.47	0.36	0.0068	3553
	2	0.47	0.36	0.0078	2335
	3	0.47	0.36	0.0097	1229
	4	0.47	0.36	0.0106	921
	5	0.47	0.36	0.0115	734
	6	0.47	0.36	0.0125	578
	7	0.47	0.36	0.0135	465
ASN3a	1	1.10	0.63	0.0073	2903
	2	1.10	0.63	0.0083	1956
	3	1.10	0.63	0.0102	1052
	4	1.10	0.63	0.0113	773
	5	1.10	0.63	0.0123	605
	6	1.10	0.63	0.0133	484
	7	1.10	0.63	0.0142	401

Table 6. Cont.

PATH	LOADING CONDITION	$\varphi_i$	$\Phi_i$	$\varepsilon_{RED,a}$	$N_{f,cal}$
		[rad]	[-]	[-]	[cycles]
ASN4	1	0.56	0.37	0.0068	3545
	2	0.56	0.37	0.0077	2453
	3	0.56	0.37	0.0097	1215
	4	0.56	0.37	0.0105	945
	5	0.56	0.37	0.0116	712
	6	0.56	0.37	0.0125	579
	7	0.56	0.37	0.0134	471
ASN5	1	0.79	0.64	0.0072	3059
	2	0.79	0.64	0.0081	2121
	3	0.79	0.64	0.0102	1055
	4	0.79	0.64	0.0111	806
	5	0.79	0.64	0.0150	344
	6	0.79	0.64	0.0131	505
	7	0.79	0.64	0.0141	405

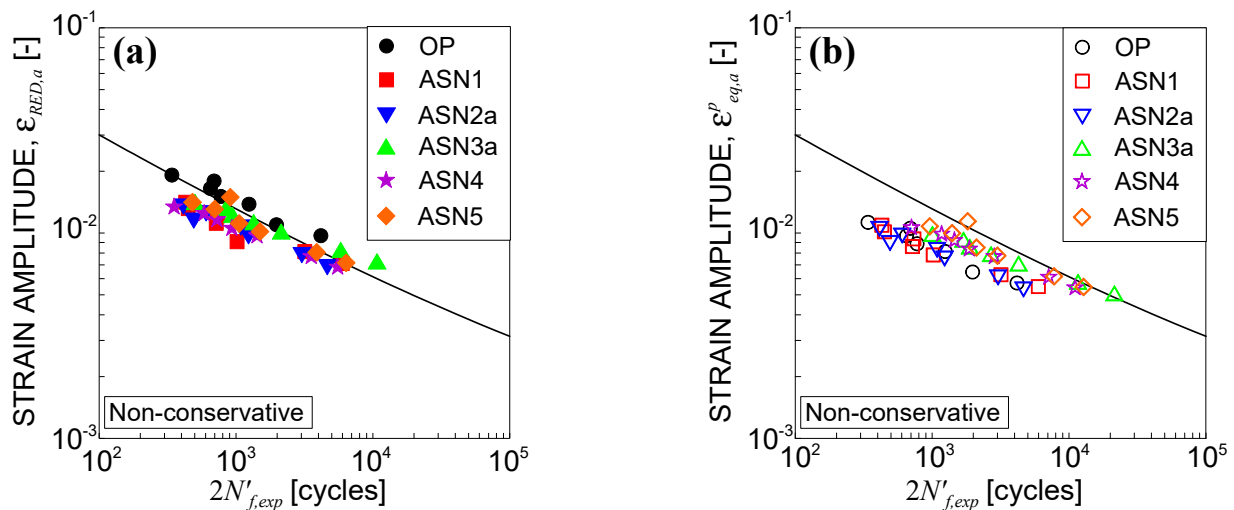
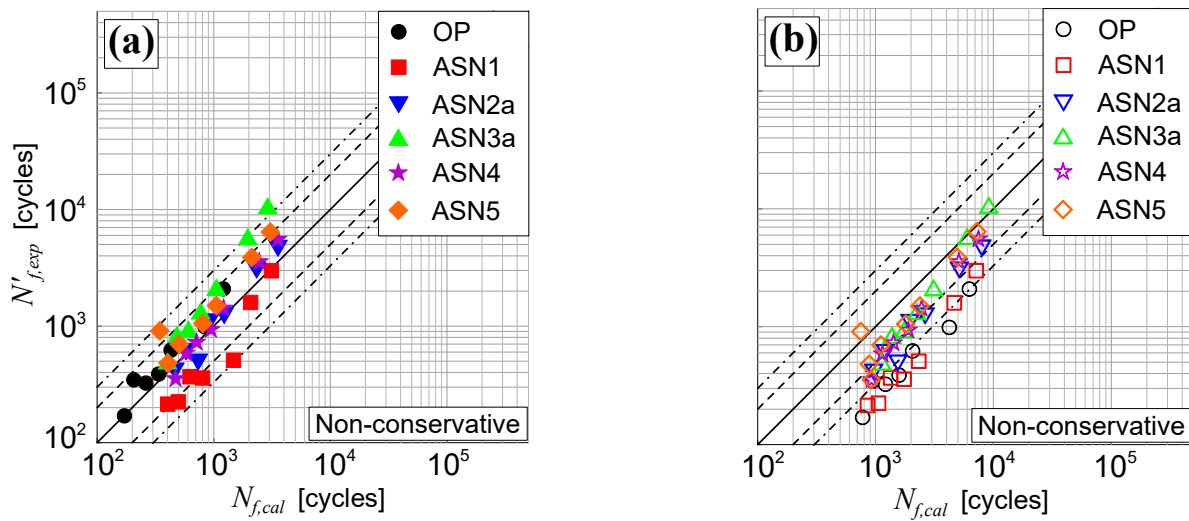


Figure 5. Correlation between the experimental fatigue life of the 304 stainless steel specimens under non-proportional loading and the strain amplitudes: (a)  $\varepsilon_{RED,a}$  (non-proportional damage parameter of the RED criterion) and (b)  $\varepsilon^p_{eq,a}$  (proportional damage parameter of Ref. [26]).

It can be noticed that, in Figure 5a, one third of the results are conservative, although also the majority of the non-conservative ones are very close to the Manson-Coffin curve. On the contrary, almost all the results determined by applying the criterion of Ref. [26] are non-conservative as shown in Figure 5b.

Figure 6 shows the correlation between the experimental fatigue life,  $N'_{f,exp}$ , and the computed one,  $N_{f,cal}$ , obtained according to both the present RED criterion (see Figure 6a) and the criterion reported in Ref. [26] (see Figure 6b).

From Figure 6a, it can be noticed that all the results obtained through the present criterion fall into the scatter band 3 (defined by the dash-dot lines), with 86% of them into the scatter band 2 (defined by the dashed lines). On the contrary, only 76% of the estimations obtained according to the criterion of Ref. [26] falls into the scatter band 3, with 31% of them into the scatter band 2 (Figure 6b). Moreover, the estimations out of the scatter band 3 lie on the non-conservative side. The accuracy of the above criteria is evaluated by means of the root mean square error  $T_{RMS}$  [26], whose values are reported in Table 7.



**Figure 6.** Correlation between the experimental fatigue life of the 304 stainless steel specimens under non-proportional loading and theoretical one computed according to: (a) the presented RED criterion and (b) the criterion of Ref. [26].

**Table 7.** Values for 304 stainless steel determined by applying the present RED criterion and the criterion of Ref. [26].

PATH	$T_{RMS}$	
	RED Criterion	Criterion of Ref. [26]
OP	1.40	3.66
ASN1	1.96	3.85
ASN2a	1.25	2.13
ASN3a	2.18	1.64
ASN4	1.29	1.89
ASN5	1.75	1.51

As can be observed, the RED criterion provides more accurate results with a  $T_{RMS} = 1.68$ , while a  $T_{RMS} = 2.47$  is achieved by applying the criterion of Ref. [26]. More in details, the best predictions are obtained for the loading paths ASN2a ( $T_{RMS} = 1.25$ ) and ASN5 ( $T_{RMS} = 1.51$ ) for the RED criterion and the criterion of Ref. [26], respectively, whereas the worst ones for the loading paths ASN3a ( $T_{RMS} = 2.18$ ) and ASN1 ( $T_{RMS} = 3.85$ ), respectively.

#### 4.1.4. Comparison with Literature Data

Finally, the results of the 304 stainless steel specimens, available in the literature [29] and obtained by using two other criteria, that is, the Fatemi and Socie (FS) [30], and the Smith, Watson, and Topper (SWT) [31,32] ones, are here compared with the estimations performed through the present RED criterion. In Figure 7, the correlation between the experimental fatigue life  $N'_{f,exp}$  and the computed one  $N_{f,cal}$  is plotted for the non-proportional loading and both FS and SWT criteria.

From Figure 7a, it can be noticed that almost all the results obtained through the FS criterion [29] fall into the scatter band 3, with 83% of them into the scatter band 2. On the other hand, 83% of the estimations obtained according to the SWT criterion [29] falls into the scatter band 3, with 53% of them into the scatter band 2 (Figure 7b). Moreover, the estimations out of the scatter band 3 lie the non-conservative side.

Regarding the accuracy, the root mean square error of the FS criterion is almost equal to that of the present criterion, that is,  $T_{RMS} = 1.65$ , whereas a slightly greater value is obtained for the SWT criterion, that is,  $T_{RMS} = 1.85$ .

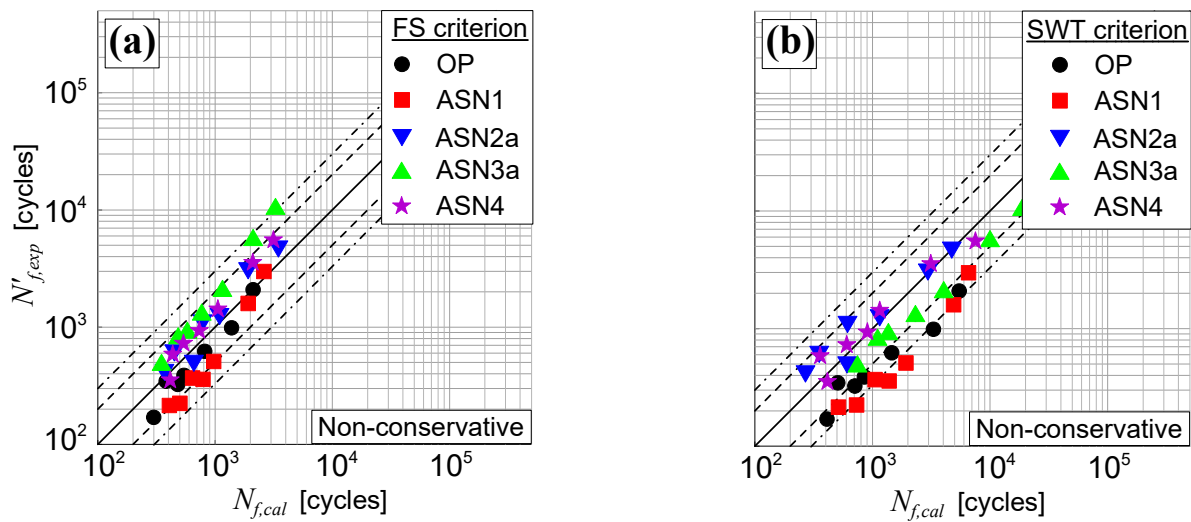


**Figure 7.** Correlation between the experimental fatigue life of the 304 stainless steel specimens under non-proportional loading and computational one available in the literature [29] and obtained according to: (a) the FS criterion and (b) the SWT criterion.

#### 4.2. 355 Structural Steel

##### 4.2.1. Material Sensitivity to Non-Proportional Loading and RED Parameter Computation

The required input data for the present RED criterion related to the 355 structural steel are listed in Table 2.  $\sigma'_f$ ,  $E$ ,  $b$ ,  $\epsilon'_f$  and  $c$  are taken from Ref. [21], whereas  $\tau'_f$  and  $\gamma'_f$  are computed as  $\tau'_f = \sigma'_f / \sqrt{3}$  and  $\gamma'_f = \epsilon'_f / \sqrt{3}$ , respectively,  $b_0 = b$  and  $c_0 = c$  are assumed, and  $G$  is determined as a function of the elastic modulus  $E$ . The fatigue strengths computed through Equations (11) by assuming  $N_0 = 2 \cdot 10^6$  loading cycles are equal to  $\sigma_{af,-1} = 254.9$  MPa and  $\tau_{af,-1} = 147.2$  MPa. The ratio  $\tau_{af,-1} / \sigma_{af,-1}$  is equal to 0.577, that is, the material is considered sensitive to non-proportional loading. Further,  $\nu_{eff}$  is taken from Ref. [16].

The computed values of  $k$  and  $\alpha$  for such a structural steel are equal to 0.1931 and 0.4051, respectively.

##### 4.2.2. Proportional Loading Tests Results

Figure 8 shows the correlation between the experimental fatigue life,  $N'_{f,exp}$ , and the computed one,  $N_{f,cal}$ , for the proportional loading IP.

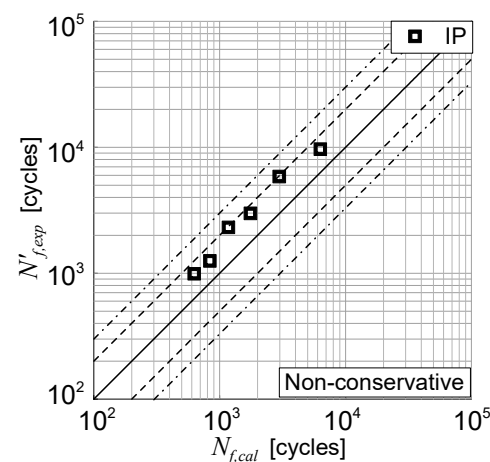


**Figure 8.** Correlation between the experimental and computational fatigue life of the 355 structural steel specimens under proportional loading.

As can be observed from Figure 8, all the results fall into the scatter band 2 (defined by the dashed lines). The accuracy of the estimations is evaluated by means of the root mean square error  $T_{RMS}$  [26], which is equal to 1.72.

#### 4.2.3. Non-Proportional Loading Tests Results

The computed values of  $\varphi_i$  and  $\Phi_i$  are listed in Table 8 for each examined non-proportional loading condition. The computed values of both  $\varepsilon_{RED,a}$  and  $N_{f,cal}$  are also listed in such a Table.

**Table 8.** 355 structural steel:  $\varphi_i$ ,  $\Phi_i$ ,  $\varepsilon_{RED,a}$  and  $N_{f,cal}$  values for each examined non-proportional loading condition.

PATH	LOADINGCONDITION	$\varphi_i$ [rad]	$\Phi_i$ [-]	$\varepsilon_{RED,a}$ [-]	$N_{f,cal}$ [cycles]
OP	1	2.37	0.62	0.0047	3683
	2	2.37	0.62	0.0059	2016
	3	2.37	0.62	0.0070	1367
	4	2.37	0.62	0.0082	949
	5	2.37	0.62	0.0095	701
	6	2.37	0.62	0.0118	448
	7	2.37	0.62	0.0131	366
ASN1	1	0.70	0.54	0.0040	5756
	2	0.70	0.54	0.0049	3184
	3	0.70	0.54	0.0059	2047
	4	0.70	0.54	0.0068	1470
	5	0.70	0.54	0.0077	1094
	6	0.70	0.54	0.0096	683
	7	0.70	0.54	0.0096	683
ASN2b	1	0.82	0.44	0.0064	1661
	2	0.82	0.44	0.0073	1254
	3	0.82	0.44	0.0091	775
	4	0.82	0.44	0.0099	645
ASN3b	1	1.10	0.36	0.0037	7233
	2	1.10	0.36	0.0054	2497
	3	1.10	0.36	0.0062	1779
	4	1.10	0.36	0.0072	1300
	5	1.10	0.36	0.0080	1025
	6	1.10	0.36	0.0089	813
ASN4	1	0.56	0.38	0.0038	6745
	2	0.56	0.37	0.0046	3886
	3	0.56	0.37	0.0054	2551
	4	0.56	0.37	0.0065	1639
	5	0.56	0.37	0.0073	1253
	6	0.56	0.37	0.0092	760
	7	0.56	0.37	0.0100	637
ASN5	1	0.79	0.64	0.0040	5680
	2	0.79	0.64	0.0050	3079
	3	0.79	0.64	0.0059	2076
	4	0.79	0.64	0.0069	1434
	5	0.79	0.64	0.0077	1102
	6	0.79	0.64	0.0097	674
	7	0.79	0.64	0.0102	607

The correlation between the experimental fatigue life  $N'_{f,exp}$  and the non-proportional damage parameter,  $\varepsilon_{RED,a}$ , are shown in Figure 9a, whereas the correlation between the experimental fatigue life  $N'_{f,exp}$  and the damage parameter of Ref. [26],  $\varepsilon_{eq,a}^p$ , is shown in Figure 9b, together with the Manson-Coffin curves (see the black solid lines).

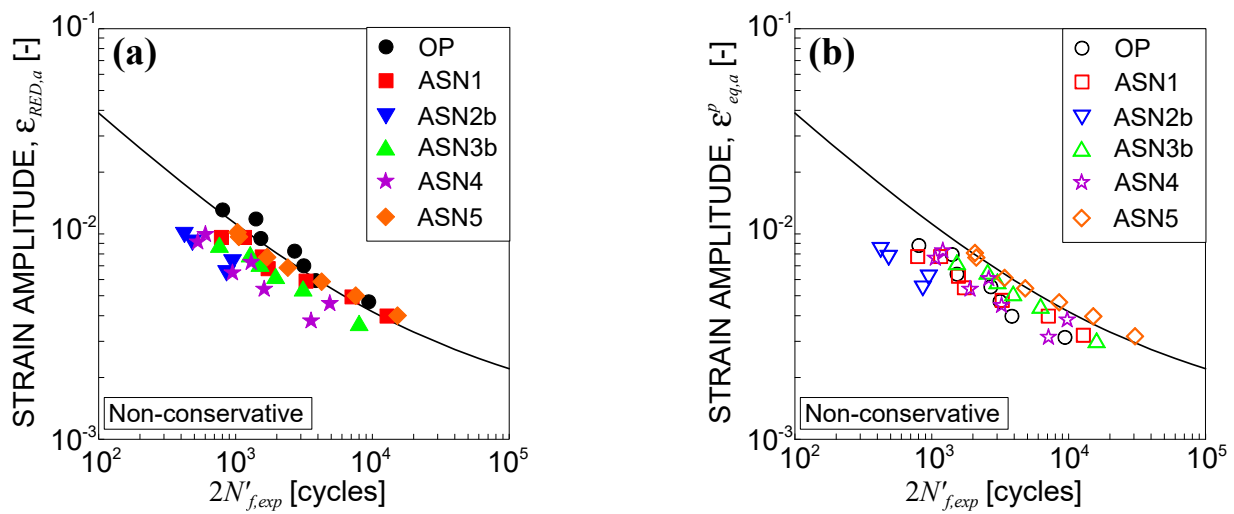


**Figure 9.** Correlation between the experimental fatigue life of the 355 structural steel specimens under non-proportional loading and the strain amplitudes: (a)  $\epsilon_{RED,a}$  (non-proportional damage parameter of the RED criterion) and (b)  $\epsilon'_{eq,a}$  (proportional damage parameter of Ref. [26]).

It can be noticed that, in Figure 9a, about one third of the results are conservative, although also the non-conservative ones (with the exception of the values related to loading paths ASN2b and ASN4) are very close to the Manson-Coffin curve. On the contrary, almost all the results determined by applying the procedure proposed in Ref. [26] are non-conservative as shown in Figure 9b.

Figure 10 shows the correlation between the experimental fatigue life,  $N'_{f,exp}$ , and the computed one,  $N'_{f,cal}$ , obtained according to both the present RED criterion (see Figure 10a) and the criterion reported in Ref. [26] (see Figure 10b).

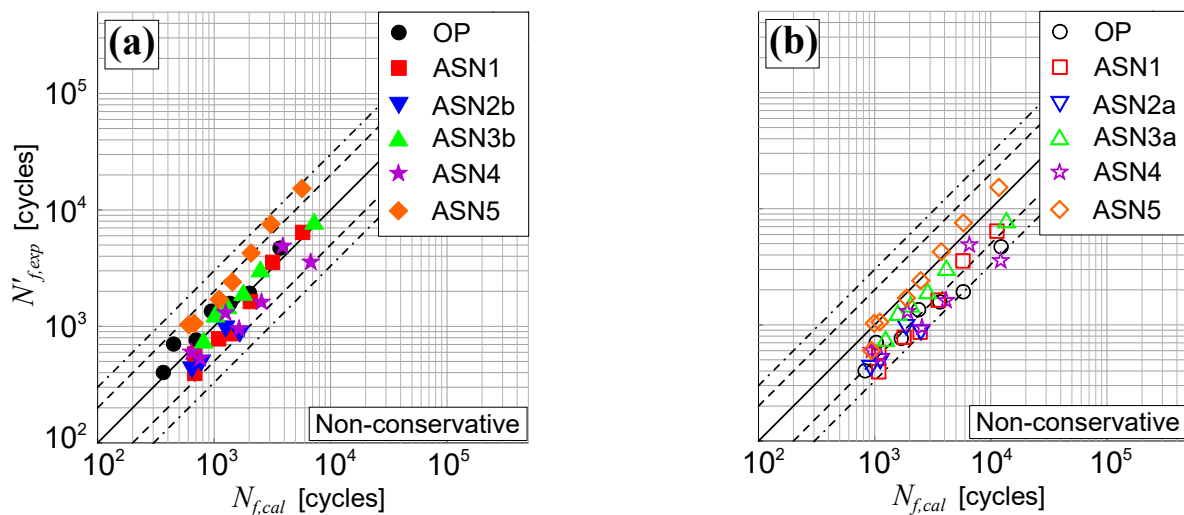


**Figure 10.** Correlation between the experimental fatigue life of the 355 structural steel specimens under non-proportional loading and theoretical one according to: (a) the present RED criterion and (b) the criterion of Ref. [26].

From Figure 10a, it can be noticed that all the results obtained through the present criterion fall into the scatter band 3 (represented by the dash-dot lines) with 92% of them into the scatter band 2 (represented by the dashed lines). On the contrary, only 61% of the estimations obtained according to the criterion of Ref. [20] falls into the scatter band 2, even if, almost all the results are within the scatter band 3 (Figure 10b).

The accuracy of the estimations is also evaluated by means of the root mean square error  $T_{RMS}$  [26], whose values are reported in Table 9 for both criteria.

**Table 9.** Values for 355 structural steel determined by applying the present RED criterion and the criterion of Ref. [26].

PATH	$T_{RMS}$	
	RED Criterion	Criterion of Ref. [26]
OP	1.28	2.22
ASN1	1.40	2.20
ASN2b	1.61	2.35
ASN3b	1.17	1.47
ASN4	1.49	2.20
ASN5	1.97	1.17

As can be observed, the RED criterion provides more accurate results with a  $T_{RMS} = 1.52$ , while a  $T_{RMS} = 1.96$  is achieved by applying the criterion of Ref. [26]. More in details, the best predictions are obtained for the loading paths ASN3b ( $T_{RMS} = 1.17$ ) and ASN5 ( $T_{RMS} = 1.17$ ) for the RED criterion and the criterion of Ref. [26], respectively, whereas the worst ones for the loading paths ASN5 ( $T_{RMS} = 1.97$ ) and ASN2b ( $T_{RMS} = 2.35$ ), respectively.

#### 4.2.4. Comparison with Literature Data

Finally, the results of the 355 structural steel specimens, available in the literature [29] and obtained by using two other criteria, that is, the Fatemi and Socie (FS) [30], and the Smith, Watson, and Topper (SWT) [31,32] ones, are here compared with the estimations performed through the present RED criterion. In Figure 11, the correlation between the experimental fatigue life  $N'_{f,exp}$  and the computed one  $N_{f,cal}$  are plotted for the non-proportional loading and both FS and SWT criteria. From Figure 11a), it can be noticed that only 16% of the results obtained through the FS criterion [29] falls into the scatter band 3 (with none of them into the scatter band 2), lying the others on the non-conservative side. For what concerns the SWT criterion [29], instead, almost all the estimations are out of the scatter band 3 on the non-conservative side (Figure 11b).

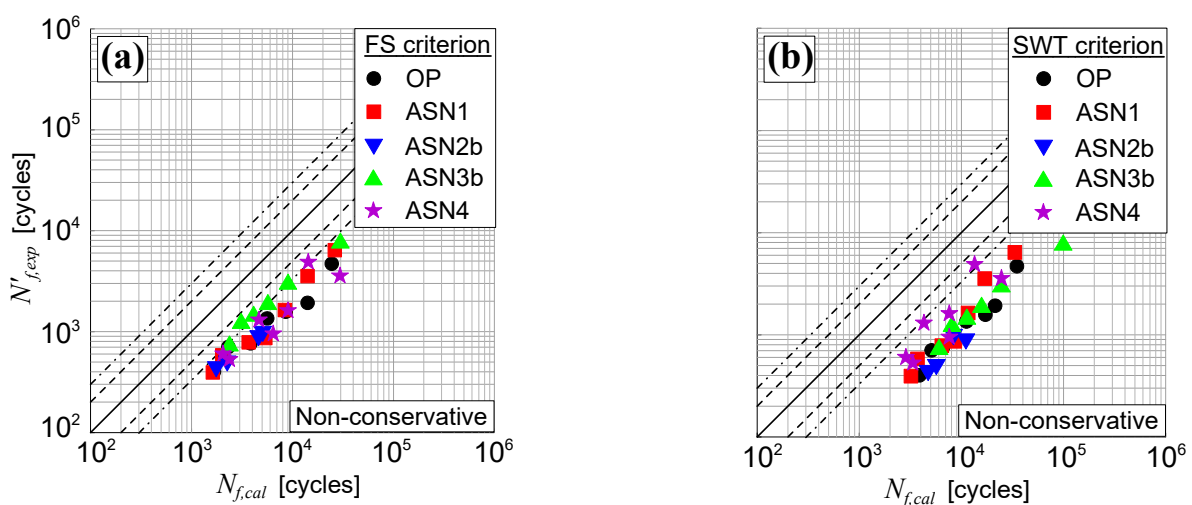


**Figure 11.** Correlation between the experimental fatigue life of the 355 structural steel specimens under non-proportional loading and theoretical one available in the literature [29] and computed according to: (a) the FS criterion and (b) the SWT criterion.

Regarding the accuracy, the root mean square error values related to both FS and SWT criteria are significantly greater ( $T_{RMS} = 3.59$  and  $T_{RMS} = 3.90$ , respectively) than the values obtained by applying the present criterion, highlighting its better accuracy.

## 5. Conclusions

In the present paper, the novel Refined Equivalent Deformation (RED) criterion has been applied for the first time to estimate the fatigue lifetime of materials, sensitive to non-proportionality, subjected to asynchronous loading under multiaxial low-cycle fatigue regime. The present criterion is complete, taking into account: (i) the strain path orientation, by means of the parameter  $\varphi_i$ , (ii) the degree of non-proportionality, by means of the parameter  $\Phi_i$ , and (iii) the changing of material cyclic properties under non-proportional loading, by means of the material constants  $k$  and  $\alpha$ .

Testing results related to two metals have been examined to evaluate the accuracy of the criterion and a comparison with results, available in the literature and obtained through two other criteria, is performed. More precisely, the accuracy of the predictions has been evaluated by both plotting the estimated and experimental fatigue lives and employing the root mean square (RMS) error method.

For the examined 304 stainless steel, it has been observed that:

- all the of the estimations fall into the scatter band 3, with 86% of them into the scatter band 2;
- the  $T_{RMS}$  value is 1.68;
- the accuracy of the RED criterion, with a  $T_{RMS} = 1.68$ , is similar to that of the Fatemi-Socie (FS) criterion ( $T_{RMS} = 1.65$ ) and slightly lower than that of the Smith, Watson and Topper (SWT) one ( $T_{RMS} = 1.85$ ).

For the examined 355 structural steel, it has been observed that:

- all the of the estimations fall into the scatter band 3, with 92% of them into the scatter band 2;
- the  $T_{RMS}$  value is 1.52;
- the accuracy of the RED criterion, with a  $T_{RMS} = 1.52$ , is significantly better than that of both the FS criterion ( $T_{RMS} = 3.59$ ) and the SWT one ( $T_{RMS} = 3.90$ ).

In conclusion, the RED criterion has been validated for non-proportionality caused by both out-of-phase and asynchronous loading and it has been demonstrated that, in comparison with other criteria available in the literature, such a criterion holds a greater accuracy.

**Funding:** This research received no external funding.

**Data Availability Statement:** Data sharing not applicable.

**Conflicts of Interest:** The author declares no conflict of interest.

## Nomenclature

$\widehat{1}, \widehat{2}, \widehat{3}$	directions of the principal strain axes at the time instant when $\varepsilon_1$ is maximum
$E$	elastic modulus
$k$	material constant representative of the material sensitivity to the change of fatigue properties
$l_i$	length of the path in the plane $\varepsilon_z - \gamma_{zt}/\sqrt{3}$
$N'_{f,exp}$	experimental number of loading cycles to failure
$N_{f,cal}$	number of loading cycles to failure
$\mathbf{w}$	normal vector to the critical plane
$rtz$	fixed frame
$S_{0,i}$	area of the smallest circle which contains the $i$ -th convex path
$S_i$	area enveloped by the $i$ -th convex path
$T_{RMS}$	root mean square error
$uvw$	local frame attached to the critical plane
$\alpha$	additional cyclic hardening coefficient
$\gamma_a$	torsional Manson–Coffin equation

$\gamma_{zt,a}$	amplitude of the applied shear strain
$\Delta$	critical plane
$\delta$	angle defining the normal to the critical plane
$\varepsilon_1, \varepsilon_2, \varepsilon_3$	principal strains
$\varepsilon_a$	tensile Manson–Coffin equation
$\varepsilon_{eq,a}^p$	equivalent deformation amplitude for proportional loading
$\varepsilon_{RED,a}$	refined equivalent deformation amplitude
$\varepsilon_{z,a}$	amplitude of the applied normal strain
$\eta$	displacement vector on the critical plane
$\eta_{N,a}$	amplitude of the normal displacement vector $\eta_N$
$\eta_{C,a}$	amplitude of the tangential displacement vector $\eta_C$
$\nu_{eff}$	effective Poisson's ratio
$\sigma_{af,-1}$	fully reversed normal strength
$\tau_{af,-1}$	fully reversed shear strength
$\Phi_i$	coefficient of non-proportionality of the $i$ -th non-proportional strain path
$\varphi_i$	angle formed by the $i$ -th non-proportional strain path with respect to the abscissa axis in the plane $\varepsilon_z - \gamma_{zt}/\sqrt{3}$

## References

- Skibicki, D. *Phenomena and Computational Models of Non-Proportional Fatigue of Materials*; Springer: London, UK, 2014.
- McDowell, D.L.; Stahl, D.R.; Stock, S.R.; Antolovich, S.D. Biaxial path dependence of deformation substructure of Type-304 Stainless-Steel. *Metall. Mater. Trans. A* **1988**, *19*, 1277–1293. [[CrossRef](#)]
- Jiao, F.; Osterle, W.; Portella, P.D.; Ziebs, J. Biaxial path-dependence of low-cycle fatigue behavior and microstructure of Alloy 800-H at room-temperature. *Mater. Sci. Eng. A* **1995**, *196*, 19–24. [[CrossRef](#)]
- Zhang, J.X.; Jiang, Y.Y. An experimental investigation on cyclic plastic deformation and substructures of polycrystalline copper. *Int. J. Plast.* **2005**, *21*, 2191–2211. [[CrossRef](#)]
- Nishino, S.; Hamada, N.; Sakane, M.; Ohnami, M.; Matsumura, N.; Tokizane, M. Microstructural study of cyclic strain-hardening behavior in biaxial stress states at elevated-temperature. *Fatigue Fract. Eng. Mater. Struct.* **1986**, *9*, 65–77. [[CrossRef](#)]
- Rios, E.R.; Andrews, R.M.; Brown, M.W.; Miller, K.J. Out-of-phase cyclic deformation and fatigue fracture studies on 316 stainless steel. In *Biaxial and Multiaxial Fatigue, EGF 3*; Mechanical Engineering Publications: London, UK, 1989.
- Bocher, L.; Delobelle, P.; Robinet, P.; Feaugas, X. Mechanical and microstructural investigations of an austenitic stainless steel under non-proportional loadings in tension-torsion-internal and external pressure. *Int. J. Plast.* **2001**, *17*, 1491–1530. [[CrossRef](#)]
- Vantadori, S. A novel multiaxial strain-based criterion considering additional cyclic hardening. *Materials* **2021**, *14*, 2542. [[CrossRef](#)]
- Ogawa, F.; Shimizu, Y.; Bressan, S.; Morishita, T.; Itoh, T. Bending and torsion fatigue-testing machine developed for multiaxial non-proportional loading. *Metals* **2019**, *9*, 1115. [[CrossRef](#)]
- Hu, D.; Pan, J.; Mi, D.; Mao, J.; Li, W.; Fu, Y.; Wang, R. Prediction of anisotropic LCF behavior for SLM Ti-6Al-4V considering the spatial orientation of defects. *Int. J. Fatigue* **2022**, *158*, 106734. [[CrossRef](#)]
- Zhan, L.; Wang, S.-Y.; Bruhns, O.T.; Xiao, H. High-efficiency algorithms for simulating metal failure effects under multiaxial repeated loadings. *Int. J. Numer. Methods Eng.* **2022**, *123*, 1277–1293. [[CrossRef](#)]
- Zhu, D.; Zhang, W.; Ding, Z. Dislocation Density Evolution in Low-Cycle Fatigue of Steels Using Dislocation-Based Crystal Plasticity. *J. Eng. Mech.* **2022**, *148*, 04021149. [[CrossRef](#)]
- Sun, T.; Xie, Y.; Pan, Y.; Zheng, Z.; Xie, C.; Huang, Z. Micromechanics-Based Low Cycle Fatigue Life Prediction Model of ECAPed Aluminum Alloy. *Metals* **2022**, *12*, 1127. [[CrossRef](#)]
- Anes, V.; Reis, L.; Freitas, M. Effect of Shear/Axial Stress Ratio on Multiaxial Non-Proportional Loading Fatigue Damage on AISI 303 Steel. *Metals* **2022**, *12*, 89. [[CrossRef](#)]
- Ellyin, F.; Gołoś, K.; Xia, Z. In phase and out-of-phase multiaxial fatigue. *J. Eng. Mater. Technol.* **1991**, *113*, 112–118. [[CrossRef](#)]
- Pejkowski, Ł.; Skibicki, D. Stress-strain response and fatigue life of four metallic materials under asynchronous loadings: Experimental observations. *Int. J. Fatigue* **2019**, *128*, 105202. [[CrossRef](#)]
- Zhou, J.; Huang, H.-Z.; Li, H. A novel energy-critical multiaxial fatigue life prediction for low cycle fatigue under mixed-mode loading. *Metals* **2018**, *8*, 1066. [[CrossRef](#)]
- Liu, J.; Zhang, Z.; Li, B.; Lang, S. Multiaxial fatigue life prediction of GH4169 alloy based on the critical plane method. *Metals* **2019**, *9*, 255. [[CrossRef](#)]
- Cruces, A.S.; Lopez-Crespo, P.; Bressan, S.; Itoh, T.; Moreno, B. On the Behaviour of 316 and 304 stainless steel under multiaxial fatigue loading: Application of the critical plane approach. *Metals* **2019**, *9*, 978. [[CrossRef](#)]
- Ronchei, C.; Carpinteri, A.; Scorza, D.; Zanichelli, A.; Vantadori, S. The RED criterion for fatigue life assessment of metals under non-proportional loading. *Int. J. Fatigue* **2022**, *163*, 107080. [[CrossRef](#)]
- Carvalho, D.; Silva, A.L.L.; Jesus, A.M.P.; Fernandes, A.A. Fatigue behaviour of structural steels. Comparison of strain-life and fatigue crack propagation data. *Mecânica Exp.* **2015**, *25*, 67–78.

22. ASTM E739-10; Standard Practice for Statistical Analysis of Linear or Linearized Stress-Life (S-N) and Strain-Life ( $\epsilon$ -N) Fatigue Data. ASTM International: West Conshohocken, PA, USA, 2015.
23. Borodii, M.V. Analysis of experimental data on low-cycle fatigue in nonproportional deformation. *Strength. Mater.* **2000**, *32*, 7–12. [[CrossRef](#)]
24. Borodii, M.V.; Strizhalo, V.A. Analysis of the experimental data on a low cycle fatigue under nonproportional straining. *Int. J. Fatigue* **2000**, *22*, 275–282. [[CrossRef](#)]
25. Borodii, M.V. Obtaining a low-cycle fatigue strain criterion. *Strength. Mater.* **2001**, *33*, 217–223. [[CrossRef](#)]
26. Vantadori, S.; Carpinteri, A.; Fortese, G.; Ronchei, C.; Scorza, D.; Zanichelli, A. Fatigue lifetime evaluation of notched components: Implementation of the control volume concept in a strain-based LCF criterion. *Theor. Appl. Fract. Mech.* **2018**, *97*, 400–408. [[CrossRef](#)]
27. Araújo, J.A.; Dantas, A.P.; Castro, F.C.; Mamiya, E.N.; Ferreira, J.L.A. On the characterization of the critical plane with a simple and fast alternative measure of the shear stress amplitude in multiaxial fatigue. *Int. J. Fatigue* **2011**, *33*, 1092–1100. [[CrossRef](#)]
28. Łagoda, T.; Kulesa, A.; Kurek, A.; Koziarska, J. Correlation of Uniaxial Cyclic Torsion and Tension-Compression for Low-Cycle Fatigue. *Mater. Sci.* **2018**, *53*, 522–531. [[CrossRef](#)]
29. Pejkowski, Ł.; Seyda, J. Fatigue of four metallic materials under asynchronous loadings: Small cracks observation and fatigue life prediction. *Int. J. Fatigue* **2021**, *142*, 105904. [[CrossRef](#)]
30. Fatemi, A.; Socie, D.F. A critical plane approach to multiaxial fatigue damage including out-of-phase loading. *Fatigue Fract. Eng. Mater. Struct.* **1988**, *11*, 149–165. [[CrossRef](#)]
31. Smith, R.N.; Watson, P.; Topper, T.H. A stress–strain parameter for the fatigue of metals. *J. Mater.* **1970**, *5*, 767–778.
32. Łagoda, T.; Vantadori, S.; Głowacka, K.; Kurek, M.; Kluger, K. Using the Smith-Watson-Topper Parameter and Its Modifications to Calculate the Fatigue Life of Metals: The State-of-the-Art. *Materials* **2022**, *15*, 3481. [[CrossRef](#)]

**Disclaimer/Publisher’s Note:** The statements, opinions and data contained in all publications are solely those of the individual author(s) and contributor(s) and not of MDPI and/or the editor(s). MDPI and/or the editor(s) disclaim responsibility for any injury to people or property resulting from any ideas, methods, instructions or products referred to in the content.